International Journal of the Physical Sciences Vol. 6(30), pp. 6801 - 6819, 23 November, 2011
Available online at http://www.academicjournals.org/IJPS
DOI: 10.5897/IJPS11.422
ISSN 1992 - 1950 ©2011 Academic Journals

Full Length Research Paper

The impact of the variability of ionospheric phase refractive index on radio signals instability

Oluseyi Ezekiel Awe[1], James A. Adegoke[2] and Babatunde Sunday Eniafe[1]*

[1]Department of Physics, University of Ibadan, Ibadan, Oyo State, Nigeria.
[2]Department of Physics, the University of Agriculture, Abeokuta, Ogun State, Nigeria.

Accepted 12 August, 2011

The ionospheric phase refractive index is a complex function that determines the attenuation and the trajectory of radio signals through the ionosphere. This complex refractive index model has been obtained using the Maxwell's equations, the tensorial conductivity equation, electron collision models, and the geomagnetic field model. The model has been used to study and investigate the phase refractive index on radio wave propagation for high latitude, low latitude and equatorial regions of the global ionosphere, at 1400 h LT, during the periods of high solar activity (Rz = 104.5, year 1970), moderate solar activity (Rz = 68.9, year 1972) and low solar activity (Rz = 12.6, year 1976). Our results showed that ionospheric phase refractive index is not constant, less than unity, increases with increasing propagating radio frequencies and for a particular propagating radio frequency, it increases with decreasing solar activity .

Key words: Ionosphere, radio signal, phase refractive index, attenuation, solar activity.

INTRODUCTION

Space communications problem is the problem of propagation through a slab of ionospheric irregularities (Liu, 1970). The variations of ionospheric parameters as a result of solar radiation affects various scientific missions involving satellites, such as communication efficiency, radar and navigation systems and forecasting of weather conditions (Habarulema, 2007; Okeke et al., 2009). Thus, in order to clearly explain what is happening in the ionosphere and give sufficient information on the impact on radio signals in the ionosphere, there is a need to understand the dynamics of the ionosphere in terms of its varying refractive index.

The ionosphere affects radio signals in different ways depending on their propagating frequencies which range from extremely low (ELF) to extremely high (EHF), oscillation frequency of the electron, the refractive index of the ionospheric plasma and the Earth's magnetic field (Budden, 1988). Due to these behaviors, the radio wave penetrates, reflects, refracts, is absorbed and delayed by the ionosphere.

The ionosphere is a dispersive medium for radio waves propagating through it. This implies that the ionospheric phase refractive index is a function of the propagating radio waves' frequency, the electron density, and to a minor degree, the intensity of the Earth's magnetic field (Langley and Komjathy, 1996). Theoretically, the concept of the phase and group velocities and phase and group refractive indices are useful for studying of the propagation of the radio waves in the ionosphere.

This research work studied and investigated the impact of the variation of the complex ionospheric refractive index on radio wave propagation in Ibadan 7.4° N, l ong 3.9° E and Dakar 14.8° N, 17.4°W (Equatorial region); Dourbes 50.1° N, l 4.6° E and Wakkanai 45.4° N, 141.7° E (Mid latitude); Tromso 69.7° N, 19.0° E and Thul e 77.5 ° N, 69.2° W (High latitude), at 1400 h LT, during the periods of high solar activity (R_Z = 104.5, year 1970), moderate solar activity (R_Z = 68.9, year 1972) and low solar activity (R_Z = 12.6, year 1976). Data sources include; IGRF Geomagnetic Field Model 1945 to 2010, International Reference Ionosphere - IRI-2007, MSIS-E-

*Corresponding author. E-mail: eniafetunde@yahoo.com. Tel: +234-702-961-3762.

90 Atmosphere Model and SPIDR. Each year for each station is classified into December solstice, March Equinox, June Solstice and September Equinox.

BASIC EQUATIONS

Ionospheric plasma

The phase refractive index of the ionosphere is a complex quantity (Ratcliffe, 1959), given as;

$$n = \mu + i\chi \quad (1)$$

μ is the real part of the ionospheric refractive index and affects the phase velocity, χ is the complex part and determines the attenuation of the wave.

The behavior of the complex refractive index of a propagation medium yields almost everything one needs to know for propagation purposes (URL-1, 1999). The ionosphere is not bound by specific, fixed limits, although the altitude at which the ionosphere begins to be detectable is about 60 km and stretches to 1200 km above the Earth's surface (URL-2, 2000; Baumjohann and Treumann, 1999). The ionosphere is a partially ionized, spherically stratified plasma with a wide spectrum of non-uniformly spaced irregularities, upon which is imposed a non-uniform magnetic field - which is itself distorted by perturbations in the solar wind (Hunsucker, 1991). The structure of the ionosphere is not constant but is continually varying in response to changes in solar radiation and the Earth's magnetic field (URL-2, 2000). The ionospheric plasma contains equal numbers of positive and negative charges (quasi-neutral) and, hence, is electrically neutral. The mass of an ion is greater than the electron mass, electrons are more mobile and thus ions have a negligible effect on radio waves (Budden, 1988). In plasmas, electrons can oscillate about the heavy ions and spiral or gyrate around the external magnetic field B_o (Davies, 1990).

The plasma oscillating angular frequency, ω_p, is given by

$$\omega_p^2 = (2\pi f_P)^2 = \frac{N_e e^2}{\varepsilon_o m_e} \quad (2)$$

The plasma angular gyrofrequency, ω_B,

$$\omega_B = 2\pi f_B = \frac{|e|}{m_e} B_o \quad (3)$$

where, N_e is the number density of electrons, e and m_e are the electron charge and mass, respectively, ε_o, is the permittivity of the free space, f_p is the plasma frequency, f_B is the plasma gyrofrequency.

Radio waves in the ionosphere are subject to some attenuation because the motions of the electrons and ions are damped through collisions with other particles (Oyinloye, 1988). When electrons in the ionosphere are set in motion by a passing wave, collisions between particles are so frequent that a major portion of their energy may be used up as heat. Changes in the index of refraction of the ionospheric medium will also cause variations in the propagation velocity and direction of propagation. This in turn will cause the energy ray paths to be delayed as it experiences refractive bending. As the electrons move under the influence of the applied electric field, they frequently collide with the more abundant neutral particles. Since the mass of an electron is thousands of times less than the mass of a neutral molecule, these collisions result in a significant loss of electron momentum and energy. The collision frequencies play a crucial role in partially ionized plasma for accurate calculations of the ionospheric refractive index and the ionospheric radio wave absorptions or attenuations. Texts by Rishbeth and Garriott (1969), Baumjohann and Treumann (1999), Siegfried (1973) and Bittencourt (1986) discuss the physics in some detail.

The motion of charged particles is strongly influenced by the presence of collisions and the electromagnetic field. Hence the equation of motion for an electron of velocity v_e under the action of the Coulomb, Lorentz forces and in the presence of collisions is (Baumjohann and Treumann, 1999).

$$m\frac{dv_e}{dt} = -e\left(\vec{E} + \vec{v_e} \times \vec{B}\right) - m_e \nu_c (v_e - u) \quad (4)$$

where $m_e \nu_c (v_e - u)$ is the collisional term, ν_e is the electron collision frequency and u is the velocity of collision targets (ions or neutrals) which will be assumed to be 0 for a steady state and ν_c is the collision frequency, given in complex form (Bittencourt, 1986) and (Rishbeth and Garriott, 1969) as;

$$\nu_c = \nu_e - i\omega = (\nu_{ei} + \nu_{en}) - i\omega \quad (5)$$

ω is signal frequency, ν_{en} is electron-neutral collisions and ν_{ei} is electron-ion collisions; Rishbeth and Garriott (1969) gave the ionospheric electron collision frequencies models as

$$\nu_{ei} = N_e \left[59 + 4.18 \log \left(\frac{Te^3}{N_e} \right) \right] \times 10^{-6} T_e^{-\frac{3}{2}} \quad (6)$$

$$\nu_{en} = 5.4 \times 10^{-16} N_n T_e^{\frac{1}{2}} \quad (7)$$

N_n is the neutral density,

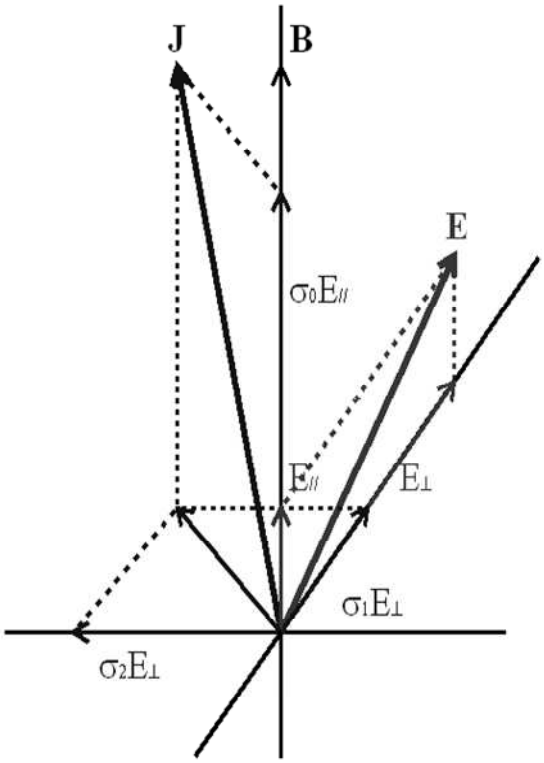

Figure 1. Relationship between electric field and current in the ionosphere (http://wdc.kugi.kyoto-u.ac.jp/ionocond/exp/figs/ejexp.gif)

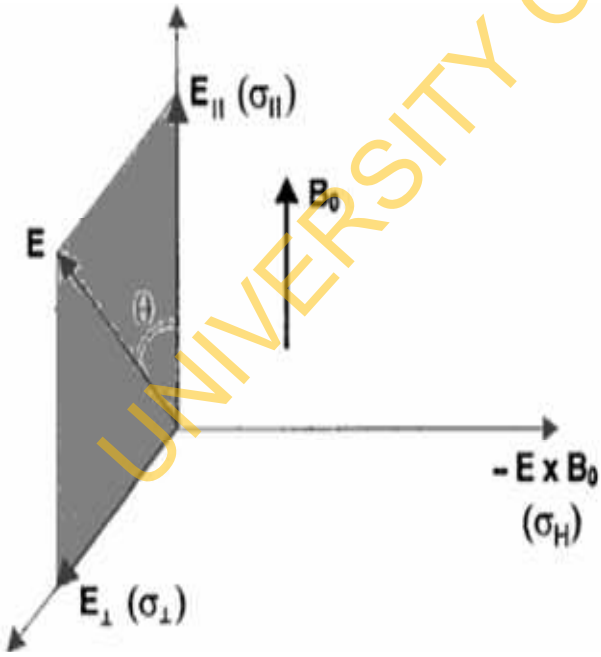

Figure 2. Relative orientation of the vector fields $E_{\parallel}$, $E_{\perp}$, and $-E \times B_0$. the conductivities $\sigma_{\parallel}$, $\sigma_{\perp}$, and σ_H govern the magnitude of the electric currents flowing along these directions, respectively (Bittencourt, 1986).

For a propagating wave in the presence of a magnetic field, it is advantageous to split the electric field vector, $\vec{E}$, into the component parallel to the magnetic field, $\vec{B}$, and the component perpendicular to magnetic field, with its respective current vectors as shown in Figure 1.

In the absence of magnetic field, B_0=0, and for a steady state (that is, $dv_e/dt = 0$), Equation (4) becomes.

$$\vec{E} = -\frac{m_e v_e (\nu_e - i\omega)}{e} \tag{8}$$

but

$$J = -en_e v_e \tag{9}$$

$$\therefore \sigma = \frac{J}{E} = \frac{n_e e^2}{m_e(\nu_e - i\omega)} = \frac{\varepsilon_o \omega_p^2}{m_e(\nu_e - i\omega)} \tag{10}$$

σ is the plasma conductivity in the absence of geomagnetic field, called the longitudinal conductivity.

Conversely, since no Lorentz forces act on a particle moving parallel to the magnetic field, the current vector can be expressed as

$$\vec{J}_{//} = \sigma_0 \vec{E}_{//} \tag{11}$$

where σ_0 is called parallel conductivity and it represents the direction parallel to the magnetic field line. This is same as that when there is no magnetic field, for this reason, σ in Equation (10) is also called the parallel conductivity given as.

$$\sigma_0 = \sigma = \frac{\varepsilon_o \omega_p^2}{m_e(\nu_e - i\omega)} \tag{12}$$

However, since the plasma may also move with velocity v_e across a magnetic field, then the $\vec{v}_e \times \vec{B}$ electric field resulting from the lorentz transformation must be added to the current equation, hence we have

$$\vec{J} = \sigma_0 \left(\vec{E} + \vec{v}_e \times \vec{B}\right) \tag{13}$$

$$\Rightarrow \vec{J} = \sigma_0 \vec{E} - \frac{\sigma_0}{n_e e} \vec{J} \times \vec{B} \qquad (J = -en_e v_e) \tag{14}$$

In solving Equation (14), we have assumed that the z-axis of the coordinate system with its origin located on the ground is vertical upwards, that is, the magnetic field is aligned with the z axis, $\vec{B} = B_0 \hat{z}$. The geometry of the geomagnetic field is thus given as shown in Figure 2.

Hence,

$$\vec{J} = \sigma_0 \vec{E} - \frac{\sigma_0 B_0}{n_e e} \vec{J} \times \hat{z} \quad (15)$$

$$\vec{J} = \sigma_0 \vec{E} - \frac{\omega_B}{(\nu_e - \iota\omega)} \vec{J} \times \hat{z} \quad (16)$$

noting that

$$\vec{J} \times \hat{z} = \vec{J}_y \hat{x} - \vec{J}_x \hat{y} \quad (17)$$

$$\Rightarrow \vec{j} = \sigma_0 \vec{E} + \frac{\omega_B}{(\nu_e - i\omega)} \left(j_y \hat{x} - j_x \hat{y} \right) \quad (18)$$

then

$$j_x = \sigma_0 E_x - \frac{\omega_B}{(\nu_e - i\omega)} j_y \quad (19)$$

$$j_y = \sigma_0 E_y + \frac{\omega_B}{(\nu_e - i\omega)} j_x \quad (20)$$

and

$$j_z = \sigma_0 E_z \quad (21)$$

substituting (20) into (19), we have

$$j_x = \sigma_0 E_x - \frac{\omega_B}{(\nu_e - i\omega)} \left[\sigma_0 E_y + \frac{\omega_B}{(\nu_e - i\omega)} j_x \right] \quad (22)$$

$$j_x = \frac{(\nu_e - i\omega)^2}{(\nu_e - i\omega)^2 + \omega_B^2} \sigma_0 E_x - \frac{(\nu_e - i\omega)\omega_B}{(\nu_e - i\omega)^2 + \omega_B^2} \sigma_0 E_y \quad (23)$$

Similarly, substituting (23) into (20), we have

$$j_y = \sigma_0 E_y + \frac{\omega_B}{(\nu_e - i\omega)} \left[\frac{(\nu_e - i\omega)^2}{(\nu_e - i\omega)^2 + \omega_B^2} \sigma_0 E_x - \frac{(\nu_e - i\omega)\omega_B}{(\nu_e - i\omega)^2 + \omega_B^2} \sigma_0 E_y \right] \quad (24)$$

$$j_y = \frac{(\nu_e - i\omega)\omega_B}{(\nu_e - i\omega)^2 + \omega_B^2} \sigma_0 E_x + \frac{(\nu_e - i\omega)^2}{(\nu_e - i\omega)^2 + \omega_B^2} \sigma_0 E_y \quad (25)$$

In matrix form, Equations (23), (25) and (21), can therefore be written as

$$\begin{pmatrix} j_x \\ j_y \\ j_z \end{pmatrix} = \sigma_0 \begin{pmatrix} \frac{(\nu_e - i\omega)^2}{(\nu_e - i\omega)^2 + \omega_B^2} & -\frac{(\nu_e - i\omega)\omega_B}{(\nu_e - i\omega)^2 + \omega_B^2} & 0 \\ \frac{(\nu_e - i\omega)\omega_B}{(\nu_e - i\omega)^2 + \omega_B^2} & \frac{(\nu_e - i\omega)^2}{(\nu_e - i\omega)^2 + \omega_B^2} & 0 \\ 0 & 0 & 1 \end{pmatrix} \begin{pmatrix} E_x \\ E_y \\ E_z \end{pmatrix} \quad (26)$$

This set of component equations can be written in dyadic notation as

$$\vec{J} = \sigma \bullet \vec{E} \quad (27)$$

where σ, is the plasma conductivity tensor in this case. For a magnetic field aligned with the z direction, the conductivity tensor reads (Baumjohann and Treumann, 1999).

$$\sigma = \begin{pmatrix} \sigma_P & -\sigma_H & 0 \\ \sigma_H & \sigma_P & 0 \\ 0 & 0 & \sigma_1 \end{pmatrix} \quad (28)$$

and the tensor elements are given by

$$\sigma_P = \frac{(\nu_e - i\omega)^2}{(\nu_e - i\omega)^2 + \omega_B^2} \sigma_0 = \frac{\varepsilon_\circ \omega_p^2 (\nu_e - i\omega)}{\left[\omega_B^2 + (\nu_e - i\omega)^2 \right]} \quad (29)$$

$$\sigma_H = \frac{(\nu_e - i\omega)\omega_B}{(\nu_e - i\omega)^2 + \omega_B^2} \sigma_0 = \frac{\varepsilon_\circ \omega_p^2 \omega_B}{\left[\omega_B^2 + (\nu_e - i\omega)^2 \right]} \quad (30)$$

$$\sigma_1 = \sigma_0 = \frac{\varepsilon_\circ \omega_p^2}{(\nu_e - i\omega)} \quad (31)$$

The tensor element σ_p is called Pedersen conductivity and governs the Pedersen current in direction of that part of the electric field, $\vec{E}_\perp$, which is transverse to the magnetic field. The Hall conductivity, σ_H, determines the Hall current in the direction perpendicular to both the electric and magnetic field, in the $-\vec{E} \times \vec{B}$ direction. The element σ_1 as earlier stated is the parallel conductivity since it governs the magnetic field-aligned current driven by the parallel electric field component $\vec{E}_{//}$ (Baumjohann and Treumann, 1999). (Recall that the parallel conductivity is equal to the plasma conductivity in the unmagnetized case).

Radio propagation through plasma

A plane wave propagating in the ionospheric plasma satisfies the following set of Maxwell's Equations (Bo Thide, 2004) and (URL-3, 2008);

$$\nabla \cdot \overline{E} = 0 \tag{32}$$

$$\nabla \cdot \overline{B} = 0 \tag{33}$$

$$\nabla \times \overline{E} = -\frac{\partial \overline{B}}{\partial t} \tag{34}$$

$$\nabla \times \overline{B} = \mu_{\circ} J + \mu_{\circ} \varepsilon_{\circ} \frac{\partial \overline{E}}{\partial t} \tag{35}$$

The electric field component a radio wave propagating in space is given by,

$$\overline{E} = \overline{E}_{\circ} \, exp\left[i\left(\overline{k}.r - \omega t\right)\right] \tag{36}$$

with similar expressions for magnetic field, $\vec{B}$, and velocity, $\vec{v}$, where ω is the angular frequency and k wave vector. In our chosen Cartesian coordinate system, we assumed that the z axis coincide with the wave normal of the plane then, the electric field component a radio wave propagating in space may be written as,

$$\overline{E}(z,t) = \overline{E}_{\circ} \, exp\left[i\left(\overline{k}z - \omega t\right)\right] \tag{37}$$

for constant phase

$$\frac{\partial z}{\partial t} = v_{ph} = \frac{\omega}{k}\hat{k} = \frac{c}{n} \tag{38}$$

where $k \equiv \left|\overline{k}\right|$ and $\hat{k}$ is a unit vector pointing in the direction of $\vec{k}$, v_{ph} is termed the phase-velocity;

$$\therefore k = \frac{\omega}{c} n \tag{39}$$

n is the phase refractive index of the propagating medium, in this case the ionospheric plasmas as given in Equation (1) and c is the speed of light in the free space. Equation (37) can therefore be written for propagation through the ionosphere as

$$\overline{E}(z,t) = \overline{E}_{\circ} \, exp\left[i\left(\frac{\omega}{c}\mu z - \omega t\right)\right].exp - \left(\frac{\omega}{c}\chi z\right) \tag{40}$$

The $\frac{\omega}{c}\chi$ term is called the absorption coefficient, κ, and this expression shows that the radio wave propagating through the ionosphere is attenuated by the term of $exp - \left(\frac{\omega}{c}\chi z\right)$. Substitution of the plane wave solution of Equation (37) into Maxwell's equations yields

$$\nabla \times \overline{E} = -\frac{\partial\left[\overline{B}_{\circ} e^{i(kz-\omega t)}\right]}{\partial t} = i\omega\overline{B} \tag{41}$$

similarly

$$\nabla \times \overline{B} = \mu_O J + \mu_O \varepsilon_O \frac{\partial\left[\overline{E}_{\circ} e^{i(k.r-\omega t)}\right]}{\partial t} = \mu_O J - i\omega\mu_O\varepsilon_O\overline{E} \tag{42}$$

Now

$$\nabla \times \left(\nabla \times \overline{E}\right) = i\omega\left(\nabla \times \overline{B}\right) \tag{43}$$

Recall

$$\nabla \times \left(\nabla \times \overline{E}\right) = \nabla\left(\nabla \cdot \overline{E}\right) - \nabla^2\overline{E} = -\nabla^2\overline{E} \tag{44}$$

$$\Rightarrow -\nabla^2\overline{E} = i\frac{\omega}{\varepsilon_O c^2} J + \frac{\omega^2}{c^2}\overline{E} \qquad \left(c = \frac{1}{\sqrt{\mu_O\varepsilon_O}}\right) \tag{45}$$

For the plane wave propagating in the z axis of assumed Cartesian coordinate, it implies that

$$\frac{\partial}{\partial x} = \frac{\partial}{\partial y} = 0 \tag{46}$$

$$\therefore \nabla = \frac{\partial}{\partial z} = ik \tag{47}$$

Equation (45) becomes

$$k^2.\overline{E} = i\frac{\omega}{\varepsilon_o c^2}\sigma.\overline{E} + \frac{\omega^2}{c^2}\overline{E} \tag{48}$$

$$\left[\frac{\omega}{c}n\right]^2.\overline{E} = i\frac{\omega}{\varepsilon_O c^2}\overline{\sigma}.\overline{E} + \frac{\omega^2}{c^2}\overline{E} \tag{49}$$

$$\Rightarrow n^2\vec{E} = \left(i\frac{\sigma}{\omega\varepsilon_o} + I\right).\vec{E} \tag{50}$$

where **I** is an identity tensor; the identity tensor takes every vector into itself and 1 is often written as the identity tensor as;

$$I = \delta_{ij} = \begin{pmatrix} 1 & 0 & 0 \\ 0 & 1 & 0 \\ 0 & 0 & 1 \end{pmatrix} \quad (51)$$

δ_{ij} is known as the kronecker delta symbol

Rearranging Equation (50), we have

$$\left[n^2 I - \left(I + i\frac{\sigma}{\omega\varepsilon_o} \right) \right].\overline{E} = 0 \quad (52)$$

Tensorially, Equation (52) can be written as

$$\overrightarrow{M} \cdot \vec{E} = 0 \quad (53)$$

where

$$\overrightarrow{M}(\omega,k) = \left[n^2 I - \left(I + i\frac{\sigma}{\omega\varepsilon_o} \right) \right] = \left(n^2 \begin{bmatrix} 1 & 0 & 0 \\ 0 & 1 & 0 \\ 0 & 0 & 1 \end{bmatrix} - \left(\begin{bmatrix} 1 & 0 & 0 \\ 0 & 1 & 0 \\ 0 & 0 & 1 \end{bmatrix} + i\frac{1}{\omega\varepsilon_o} \begin{bmatrix} \sigma_P & \sigma_H & 0 \\ -\sigma_H & \sigma_P & 0 \\ 0 & 0 & \sigma_1 \end{bmatrix} \right) \right) \quad (54)$$

In tensor form, Equation (53) becomes

$$\begin{bmatrix} M_{xx} & M_{xy} & M_{xz} \\ M_{yx} & M_{yy} & M_{yz} \\ M_{zx} & M_{zy} & M_{zz} \end{bmatrix} \cdot \begin{bmatrix} E_x \\ E_y \\ E_z \end{bmatrix} = 0 \quad (55)$$

where

$$\left.\begin{aligned} M_{xx} &= M_{yy} = n^2 - 1 - \frac{i\sigma_P}{\varepsilon_O\omega} \\ M_{xy} &= -M_{yx} = -\frac{i\sigma_H}{\varepsilon_O\omega} \\ M_{xz} &= M_{yz} = M_{zx} = M_{zy} = 0 \\ M_{zz} &= -1 - \frac{i\sigma_1}{\varepsilon_O\omega} \end{aligned}\right\} \quad (56)$$

Determinant $|M| = o$ is called the basic dispersion relation.

Therefore, replacing the tensor elements, the dispersion relation is

$$\begin{vmatrix} M_{xx} & M_{xy} & 0 \\ M_{yx} & M_{yy} & 0 \\ 0 & 0 & M_{zz} \end{vmatrix} = 0 \quad (57)$$

The complex refractive index n can be obtained in terms of plasma parameters by solving the dispersion relation. Thus

$$\begin{vmatrix} M_{xx} & M_{xy} & 0 \\ M_{yx} & M_{yy} & 0 \\ 0 & 0 & M_{zz} \end{vmatrix} = M_{xx}M_{yy}M_{zz} + M_{xy}M_{yx}M_{zz} = 0 \quad (58)$$

$$\therefore M_{zz}\left(M_{xx}^2 - M_{xy}^2\right) = M_{zz}\left(M_{xx} + M_{xy}\right)\left(M_{xx} + M_{xy}\right) = 0 \quad (59)$$

Substituting respective components of Equation (56), we have

$$\left(-1 - \frac{i\sigma_1}{\varepsilon_\circ\omega}\right)\left(n^2 - 1 - \frac{i\sigma_P}{\varepsilon_\circ\omega} - \frac{\sigma_H}{\varepsilon_\circ\omega}\right)\left(n^2 - 1 - \frac{i\sigma_P}{\varepsilon_\circ\omega} + \frac{\sigma_H}{\varepsilon_\circ\omega}\right) = 0 \quad (60)$$

This is a quadratic equation in terms of *n*; the first expression is the plasma oscillation, the second expression is the left-hand polarized wave and the third expression is the right-hand polarized wave. Considering only the left-hand polarized wave,

$$\Rightarrow n^2 - 1 = \frac{i\sigma_P}{\varepsilon_\circ\omega} - \frac{\sigma_H}{\varepsilon_\circ\omega} \quad (61)$$

$$\therefore n^2 - 1 = i\frac{\omega_p^2(\nu_e - i\omega)}{\omega\left[\omega_B^2 + (\nu_e - i\omega)^2\right]} - \frac{\omega_p^2\omega_B}{\omega\left[\omega_B^2 + (\nu_e - i\omega)^2\right]} = \frac{i\left(\omega_p^2(\nu_e - i\omega)\right) - \omega_p^2\omega_B}{\omega\left[\omega_B^2 + \nu_e^2 - \omega^2 - i2\nu_e\omega\right]} \quad (62)$$

Rationalizing the complex fraction, we have

$$n^2 - 1 = \frac{\left[i\left(\omega_p^2(\nu_e - i\omega)\right) - \omega_p^2\omega_B\right]\left[\omega_B^2 + \nu_e^2 - \omega^2 + i2\nu_e\omega\right]}{\omega\left[\omega_B^2 + \nu_e^2 - \omega^2 - i2\nu_e\omega\right]\left[\omega_B^2 + \nu_e^2 - \omega^2 + i2\nu_e\omega\right]} \quad (63)$$

$$n^2 - 1 = \frac{i\omega_p^2\nu_e\left(\omega_B^2 + \nu_e^2 - \omega^2\right) + \omega_p^2\omega\left(\omega_B^2 + \nu_e^2 - \omega^2\right) + i2\omega_p^2\omega^2\nu_e - 2\omega_p^2\omega\nu_e^2 - \omega_p^2\omega_B\left(\omega_B^2 + \nu_e^2 - \omega^2\right) - i2\omega_p^2\omega_B\omega\nu_e}{\omega\left[\left(\omega_B^2 + \nu_e^2 - \omega^2\right)^2 + 4\nu_e^2\omega^2\right]} \quad (64)$$

separating into real and imaginary parts, we have

$$\therefore n^2 = 1+\frac{\omega_p^2}{\omega}\left[\frac{(\omega-\omega_B)(\omega_B^2+\nu_e^2-\omega^2)-2\omega\nu_e^2}{(\omega_B^2+\nu_e^2-\omega^2)^2+4\omega^2\nu_e^2}\right]+i\frac{\omega_p^2}{\omega}\left[\frac{2\omega\nu_e^2(\omega-\omega_B)+\nu_e(\omega_B^2+\nu_e^2-\omega^2)}{(\omega_B^2+\nu_e^2-\omega^2)^2+4\omega^2\nu_e^2}\right] \quad (65)$$

$$\Rightarrow n^2 = M + iN \quad (66)$$

where

$$M = 1+\frac{\omega_p^2}{\omega}\left[\frac{(\omega-\omega_B)(\omega_B^2+\nu_e^2-\omega^2)-2\omega\nu_e^2}{(\omega_B^2+\nu_e^2-\omega^2)^2+4\omega^2\nu_e^2}\right] \quad (67)$$

$$N = \frac{\omega_p^2}{\omega}\left[\frac{2\omega\nu_e^2(\omega-\omega_B)+\nu_e(\omega_B^2+\nu_e^2-\omega^2)}{(\omega_B^2+\nu_e^2-\omega^2)^2+4\omega^2\nu_e^2}\right] \quad (68)$$

Equation (1) can therefore be written as;

$$n^2 = (\mu+i\chi)^2 = M+iN \quad (69)$$

that is,

$$n = (\mu+i\chi) = \sqrt{(M+iN)} \quad (70)$$

to solve μ and χ recall from complex analysis that if

$$z = x+iy \quad (71)$$

that

$$\sqrt{z} = \pm\left[\left(\frac{|z|+M}{2}\right)^{\frac{1}{2}}+i\left(\frac{|z|+M}{2}\right)^{\frac{1}{2}}\right] \quad (72)$$

$$\Rightarrow \mu = \pm\left(\frac{(M^2+N^2)^{\frac{1}{2}}+M}{2}\right)^{\frac{1}{2}} \quad (73)$$

and

$$\chi = \pm\left(\frac{(M^2+N^2)^{\frac{1}{2}}-M}{2}\right)^{\frac{1}{2}} \quad (74)$$

Therefore the theoretical model for the complex phase refractive index of the ionospheric plasmas is

$$n = \mu+i\chi = \pm\left[\left(\frac{(M^2+N^2)^{\frac{1}{2}}+M}{2}\right)^{\frac{1}{2}}+i\left(\frac{(M^2+N^2)^{\frac{1}{2}}-M}{2}\right)\right] \quad (75)$$

$$\mathbf{n} = \pm\left(\frac{\left(\left(1+\frac{\omega_p^2}{\omega}\left[\frac{(\omega-\omega_B)(\omega_B^2+\nu_e^2-\omega^2)-2\omega\nu_e^2}{(\omega_B^2+\nu_e^2-\omega^2)^2+4\omega^2\nu_e^2}\right]\right)^2+\left(\frac{\omega_p^2}{\omega}\left[\frac{2\omega\nu_e^2(\omega-\omega_B)+\nu_e(\omega_B^2+\nu_e^2-\omega^2)}{(\omega_B^2+\nu_e^2-\omega^2)^2+4\omega^2\nu_e^2}\right]\right)^2\right)^{\frac{1}{2}}+\left(1+\frac{\omega_p^2}{\omega}\left[\frac{(\omega-\omega_B)(\omega_B^2+\nu_e^2-\omega^2)-2\omega\nu_e^2}{(\omega_B^2+\nu_e^2-\omega^2)^2+4\omega^2\nu_e^2}\right]\right)}{2}\right)$$
$$+i\left(\frac{\left(\left(1+\frac{\omega_p^2}{\omega}\left[\frac{(\omega-\omega_B)(\omega_B^2+\nu_e^2-\omega^2)-2\omega\nu_e^2}{(\omega_B^2+\nu_e^2-\omega^2)^2+4\omega^2\nu_e^2}\right]\right)^2+\left(\frac{\omega_p^2}{\omega}\left[\frac{2\omega\nu_e^2(\omega-\omega_B)+\nu_e(\omega_B^2+\nu_e^2-\omega^2)}{(\omega_B^2+\nu_e^2-\omega^2)^2+4\omega^2\nu_e^2}\right]\right)^2\right)^{\frac{1}{2}}-\left(1+\frac{\omega_p^2}{\omega}\left[\frac{(\omega-\omega_B)(\omega_B^2+\nu_e^2-\omega^2)-2\omega\nu_e^2}{(\omega_B^2+\nu_e^2-\omega^2)^2+4\omega^2\nu_e^2}\right]\right)}{2}\right) \quad (76)$$

The plus and minus signs correspond to the ordinary and extraordinary wave modes of propagation and the plane wave propagating through the ionospheric plasmas for the ordinary wave can therefore be expressed as

$$\overline{E}(z,t) = \overline{E}_\circ \exp\left[i\left(\frac{\omega}{c}\left(\left(\frac{(M^2+N^2)^{\frac{1}{2}}+M}{2}\right)^{\frac{1}{2}}\right)z-\omega t\right)\right].\exp\left(-\left(\frac{\omega}{c}\left(\left(\frac{(M^2+N^2)^{\frac{1}{2}}-M}{2}\right)\right)z\right)\right) \quad (77)$$

Hence the attenuation term can be expressed as

$$e^{-\frac{\omega}{c}\left[\pm\left(\frac{(M^2+N^2)^{\frac{1}{2}}-M}{2}\right)^{\frac{1}{2}}\cdot Z\right]} \quad (78)$$

and the phase velocity term is a function of

$$e^{i\left(\frac{\omega}{c}\left(\left(\frac{(M^2+N^2)^{\frac{1}{2}}+M}{2}\right)^{\frac{1}{2}}\right).z-wt\right)} \quad (79)$$

RESULTS AND DISCUSSION

Equation (76) shows that the refractive index is a function of the following ionospheric variables

$$n_{ph} = f\left(h,\omega,\omega_p,\omega_B,\nu_e,N_e,N_{n,}T_e,T_{n,}\sigma\right) \quad (80)$$

where, ω is angular frequency of the propagating radio signal through the ionospheric plasma

$$\omega_p = f\left(f_P\right) = f\left(N_e(h),e,\varepsilon_o,m_e\right) \quad (81)$$

$$\omega_B = f\left(f_B\right) = f\left(B_o(h),e,m_e\right) \quad (82)$$

$$\nu_e = f\left(N_e(h),N_n(h),T_e(h),T_n(h)\right) \quad (88)$$

$$\sigma = f\left(\sigma_1(h),\sigma_P(h),\sigma_H(h)\right) \quad (84)$$

h = ionospheric alttitude; D region is 60 to 80 km, E region is 85 to 110 km, F region is 115 to 440 km and TOPSIDE region is 445 to 600 km .We have assumed the ionospheric plasmas to be stratified into spherical layers, an interval of 5 km from the D region to the TOPSIDE region was considered in our computation using Microsoft Excel spreedsheet for each of the varying ionospheric parameter at 1400 LT.

Our results show that phase refractive index is less than unity for 5 MHz, 15 MHz, 25 MHz, 100 MHz, and 1.5 GHz propagating frequencies. This implies that the phase velocity is greater than the speed of light, a result already obtained by different researchers but with the exclusion of collision frequencies, ionospheric conductivities and Earth's magnetic field (Oyinloye, 1975; Bassiri and Hajj, 1993; Komjathy**,** 1997; Habarulema, 2007; Kintner and Ledvina, 2004; URL-2, 2000; Aydodu and Ozcan, 1996). Table 1 shows the phase refractive index calculated for Ibadan for the propagating frequencies, similar results were calculated for the other stations. The variation of phase refractive index with altitude explains the nature of the trajectory of radio signals in the ionosphere and as well as the delay experienced. The decreasing phase refractive index with altitude for radio signal implies a bending away from the normal and hence the reflective ability of the ionosphere for HF signals as deduced from Figures 3 to 5, and an increasing refractive index with altitude implies bending towards the normal. Therefore, a radio signal passing through the ionosphere will experience an alteration in velocity of propagation and as well as the direction of propagation; HF signals experience immense refractivity and reflected, while VHF experience double ray path alteration; to and from satellite as they pass through the ionosphere in Figure 6. The phase refractive has its minimum value around hmF_2**.**

Figures 3 to 5 show that in Ibadan for different propagating radio frequencies, the phase refractive index increases with increasing propagating radio frequencies. Also for a particular propagating radio frequency, the phase refractive index increases with decreasing solar activity as shown in Figures 7 to 9 for the different stations. The phase refractive index ranges for 5 MHz from 0.801736853 to 0.999999945, 0.679103281 to 0.999999869, and 0.58322336 to 0.99999913 for low, moderate and high solar activity respectively for all the stations as shown in Table 2. Prior to reflection, as shown in Figures 7 to 9, 5 MHz frequency and other HF radio signals in the equatorial regions will reflect (as these have very low refractive index) at a lower altitude compared with mid and high latitude regions. Therefore HF radio signals in the mid and high latitude regions will travel a wider distance for sky wave communications.

Figures 10 to 14 show the amount of energy of radio signals attenuated in the ionosphere deduced from the imaginary part of the theoretical model. It shows that attenuation increases directly with increasing solar activity, highest in D regions, very high at high solar activity a, very high at June solstice, very high for HF frequency and extremely low attenuation for VHF. These results are in agreement with that obtained by Unal et al. (2007). Furthermore, radio signals in the ionosphere are calculated to be completely attenuated for LF. Tables 3 to 5 summarized the results for calculated attenuations.

However, if the collision frequencies and the Earth's magnetic field are neglected in Equation (65), the phase refractive index becomes real and reduces to the approximated Appleton-Hartree equation, which has been used by various authors (Oyinloye, 1975; Bassiri and Hajj, 1993; Komjathy**,** 1997; Habarulema, 2007; Kintner and Ledvina, 2004; URL-2, 2000; Aydodu and Ozcan, 1996). Thus the approximated AH equation for the phase refractive index is

$$n \approx 1 - \frac{\omega_p^2}{2\omega^2} \quad (85)$$

Figure 15 shows the behaviour of the phase refractive index for the AH model and the theoretical model for 5 MHz for January 1970 at Ibadan. Figure 16 shows the variation of the amplitude attenuation of 1 V/m with altitude for 5 MHz for January 1970 for the theoretical model and AH model at Ibadan. It also shows the exclusion of the Earth's magnetic field and the electron-ion collision frequency in the theoretical model.

Conclusion

The trajectory of radio signals through the ionosphere and ionospheric phenomena like attenuation, ionospheric delay, refraction, reflection and transmission can be

Table 1. Calculated phase refractive index for Ibadan January 1970 at 1400 LT.

Layer	Altitude (km)	IBD_5 MHZ	IBD_15 MHZ	IBD_25 MHZ	IBD_100 MHZ	IBD_1.5 GHZ
D	60	0.9999511343	0.9999905509	0.9999977325	0.9999999238	0.9999999997
D	65	0.9999290078	0.9999942924	0.9999986073	0.9999999281	0.9999999997
D	70	0.9996793735	0.9999864647	0.9999956442	0.9999997140	0.9999999987
D	75	0.9994238990	0.9999794961	0.9999922071	0.9999994491	0.9999999974
D	80	0.9994842534	0.9999753706	0.9999901977	0.9999992956	0.9999999967
E	85	0.9994673652	0.9999522461	0.9999808115	0.9999986169	0.9999999935
E	90	0.9963861674	0.9994885191	0.9997941661	0.9999851604	0.9999999307
E	95	0.9892573018	0.9982478258	0.9992950652	0.9999492009	0.9999997629
E	100	0.9828276910	0.9971250505	0.9988439413	0.9999167359	0.9999996115
E	105	0.9805463705	0.9967312371	0.9986860306	0.9999054010	0.9999995586
E	110	0.9803372701	0.9966953979	0.9986719440	0.9999044195	0.9999995541
F1	115	0.9802835205	0.9966880136	0.9986692863	0.9999042603	0.9999995534
F1	120	0.9798255157	0.9966138641	0.9986398376	0.9999021755	0.9999995437
F1	125	0.9793501825	0.9965370769	0.9986093450	0.9999000171	0.9999995337
F1	130	0.9788528704	0.9964568003	0.9985774676	0.9998977606	0.9999995233
F1	135	0.9783361300	0.9963734502	0.9985443733	0.9998954182	0.9999995124
F1	140	0.9777960510	0.9962863845	0.9985098056	0.9998929716	0.9999995011
F1	145	0.9772312376	0.9961953830	0.9984736776	0.9998904146	0.9999994892
F1	150	0.9766402762	0.9961002250	0.9984359021	0.9998877411	0.9999994768
F1	155	0.9760204519	0.9960004767	0.9983963066	0.9998849389	0.9999994638
F1	160	0.9753677367	0.9958954902	0.9983546333	0.9998819896	0.9999994501
F1	165	0.9746806513	0.9957850412	0.9983107942	0.9998788870	0.9999994358
F1	170	0.9739538180	0.9956682660	0.9982644454	0.9998756067	0.9999994205
F1	175	0.9731844058	0.9955447242	0.9982154129	0.9998721364	0.9999994045
F1	180	0.9723669554	0.9954135474	0.9981633519	0.9998684517	0.9999993874
F1	185	0.9714933485	0.9952734375	0.9981077459	0.9998645158	0.9999993691
F1	190	0.9705579479	0.9951235151	0.9980482473	0.9998603041	0.9999993496
F1	195	0.9695486637	0.9949618415	0.9979840840	0.9998557618	0.9999993285
F2	200	0.9684517569	0.9947862403	0.9979143922	0.9998508274	0.9999993056
F2	205	0.9672534924	0.9945945401	0.9978383098	0.9998454400	0.9999992806
F2	210	0.9659254603	0.9943822049	0.9977540321	0.9998394709	0.9999992529
F2	215	0.9644360037	0.9941442328	0.9976595737	0.9998327794	0.9999992219
F2	220	0.9627308072	0.9938719816	0.9975514972	0.9998251209	0.9999991864
F2	225	0.9607170926	0.9935507361	0.9974239521	0.9998160795	0.9999991444
F2	230	0.9582126660	0.9931517300	0.9972655008	0.9998048417	0.9999990922
F2	235	0.9551618738	0.9926719255	0.9970749751	0.9997913272	0.9999990295
F2	240	0.9520006363	0.9921677762	0.9968748952	0.9997771429	0.9999989636
F2	245	0.9486742688	0.9916394104	0.9966653280	0.9997622947	0.9999988947
F2	250	0.9451647370	0.9910867615	0.9964462603	0.9997467823	0.9999988227
F2	255	0.9414867306	0.9905101643	0.9962178427	0.9997306177	0.9999987477
F2	260	0.9376373338	0.9899093178	0.9959799716	0.9997137945	0.9999986697
F2	265	0.9336170816	0.9892845878	0.9957328063	0.9996963247	0.9999985887
F2	270	0.9294258372	0.9886363051	0.9954764969	0.9996782204	0.9999985047
F2	275	0.9250650970	0.9879650458	0.9952112872	0.9996594995	0.9999984179
F2	280	0.9205374473	0.9872715856	0.9949375027	0.9996401864	0.9999983284
F2	285	0.9158443188	0.9865565063	0.9946553887	0.9996202992	0.9999982362
F2	290	0.9109926815	0.9858212558	0.9943655342	0.9995998806	0.9999981416
F2	295	0.9059836936	0.9850664006	0.9940681804	0.9995789486	0.9999980446
F2	300	0.9008289493	0.9842940685	0.9937641817	0.9995575645	0.9999979455
F2	305	0.8955326612	0.9835052748	0.9934539546	0.9995357585	0.9999978445
F2	310	0.8901053651	0.9827019471	0.9931382709	0.9995135858	0.9999977418

Table 1. Cont'd.

F2	315	0.8845576816	0.9818860104	0.9928179013	0.9994911013	0.9999976377
F2	320	0.8789032655	0.9810598242	0.9924937877	0.9994683722	0.9999975325
F2	325	0.8731548656	0.9802255558	0.9921667919	0.9994454598	0.9999974265
F2	330	0.8673291550	0.9793858642	0.9918379617	0.9994224378	0.9999973200
F2	335	0.8614420635	0.9785433335	0.9915083247	0.9993993794	0.9999972133
F2	340	0.8555131398	0.9777008963	0.9911790271	0.9993763645	0.9999971069
F2	345	0.8495640326	0.9768618300	0.9908513631	0.9993534850	0.9999970011
F2	350	0.8436216561	0.9760299752	0.9905268305	0.9993308453	0.9999968964
F2	355	0.8376864327	0.9752053715	0.9902054381	0.9993084456	0.9999967929
F2	360	0.8318221197	0.9743969523	0.9898906815	0.9992865313	0.9999966917
F2	365	0.8260150150	0.9736025841	0.9895817085	0.9992650413	0.9999965924
F2	370	0.8203307780	0.9728312273	0.9892820183	0.9992442209	0.9999964963
F2	375	0.8147737430	0.9720830573	0.9889916508	0.9992240710	0.9999964033
F2	380	0.8093793595	0.9713626094	0.9887123654	0.9992047142	0.9999963140
F2	385	0.8041682579	0.9706722444	0.9884450618	0.9991862123	0.9999962287
F2	390	0.7991949399	0.9700188268	0.9881923954	0.9991687498	0.9999961482
F2	395	0.7944821463	0.9694047793	0.9879552803	0.9991523886	0.9999960728
F2	400	0.7900521607	0.9688324767	0.9877346177	0.9991371904	0.9999960028
F2	405	0.7859284163	0.9683043547	0.9875313248	0.9991232173	0.9999959385
F2	410	0.7821679582	0.9678273120	0.9873480627	0.9991106538	0.9999958808
F2	415	0.7787774785	0.9674015171	0.9871848667	0.9990995004	0.9999958296
F2	420	0.7758156699	0.9670339468	0.9870444180	0.9990899422	0.9999957857
F2	425	0.7732712278	0.9667224776	0.9869258651	0.9990819181	0.9999957490
F2	430	0.7711847579	0.9664717957	0.9868310030	0.9990755514	0.9999957200
F2	435	0.7695966979	0.9662865911	0.9867616284	0.9990709658	0.9999956992
F2	440	0.7685299980	0.9661693163	0.9867186656	0.9990682235	0.9999956869
TOPSIDE	445	0.7680233931	0.9661246249	0.9867039041	0.9990674478	0.9999956838
TOPSIDE	450	0.7684677948	0.9662026674	0.9867367928	0.9990699918	0.9999956960
TOPSIDE	455	0.7700046119	0.9664217440	0.9868244242	0.9990763482	0.9999957258
TOPSIDE	460	0.7725092746	0.9667661478	0.9869606827	0.9990860881	0.9999957713
TOPSIDE	465	0.7758878142	0.9672245584	0.9871411805	0.9990989046	0.9999958310
TOPSIDE	470	0.7799925424	0.9677788179	0.9873588790	0.9991143069	0.9999959026
TOPSIDE	475	0.7847279085	0.9684175554	0.9876093792	0.9991319879	0.9999959847
TOPSIDE	480	0.7899645351	0.9691248625	0.9878865176	0.9991515179	0.9999960754
TOPSIDE	485	0.7956252787	0.9698915826	0.9881867600	0.9991726512	0.9999961735
TOPSIDE	490	0.8015834581	0.9707017698	0.9885039276	0.9991949575	0.9999962770
TOPSIDE	495	0.8077659040	0.9715463010	0.9888344889	0.9992181911	0.9999963847
TOPSIDE	500	0.8140843191	0.9724137898	0.9891740277	0.9992420443	0.9999964953
TOPSIDE	505	0.8204693327	0.9732951319	0.9895190106	0.9992662714	0.9999966076
TOPSIDE	510	0.8268869116	0.9741857961	0.9898676762	0.9992907494	0.9999967211
TOPSIDE	515	0.8332698765	0.9750766494	0.9902164780	0.9993152318	0.9999968345
TOPSIDE	520	0.8395705772	0.9759609342	0.9905627770	0.9993395344	0.9999969471
TOPSIDE	525	0.8457577735	0.9768340981	0.9909047993	0.9993635337	0.9999970583
TOPSIDE	530	0.8518045324	0.9776920716	0.9912409536	0.9993871190	0.9999971675
TOPSIDE	535	0.8576989618	0.9785328284	0.9915704435	0.9994102347	0.9999972746
TOPSIDE	540	0.8634181594	0.9793527589	0.9918918539	0.9994327821	0.9999973790
TOPSIDE	545	0.8689539324	0.9801502941	0.9922045647	0.9994547180	0.9999974806
TOPSIDE	550	0.8742949687	0.9809234125	0.9925077787	0.9994759869	0.9999975790
TOPSIDE	555	0.8794397411	0.9816714675	0.9928012328	0.9994965701	0.9999976743
TOPSIDE	560	0.8843827326	0.9823933074	0.9930844737	0.9995164365	0.9999977663
TOPSIDE	565	0.8891269328	0.9830889626	0.9933575030	0.9995355861	0.9999978549
TOPSIDE	570	0.8936735442	0.9837582324	0.9936202328	0.9995540124	0.9999979402

Table 1. Cont'd.

TOPSIDE	575	0.8980245091	0.9844010952	0.9938726518	0.9995717153	0.9999980221
TOPSIDE	580	0.9021838037	0.9850177996	0.9941148486	0.9995887007	0.9999981007
TOPSIDE	585	0.9061596131	0.9856092545	0.9943471728	0.9996049931	0.9999981761
TOPSIDE	590	0.9099539365	0.9861754755	0.9945696236	0.9996205923	0.9999982483
TOPSIDE	595	0.9135742052	0.9867173418	0.9947825435	0.9996355228	0.9999983173
TOPSIDE	600	0.9170282105	0.9872357701	0.9949862853	0.9996498090	0.9999983834

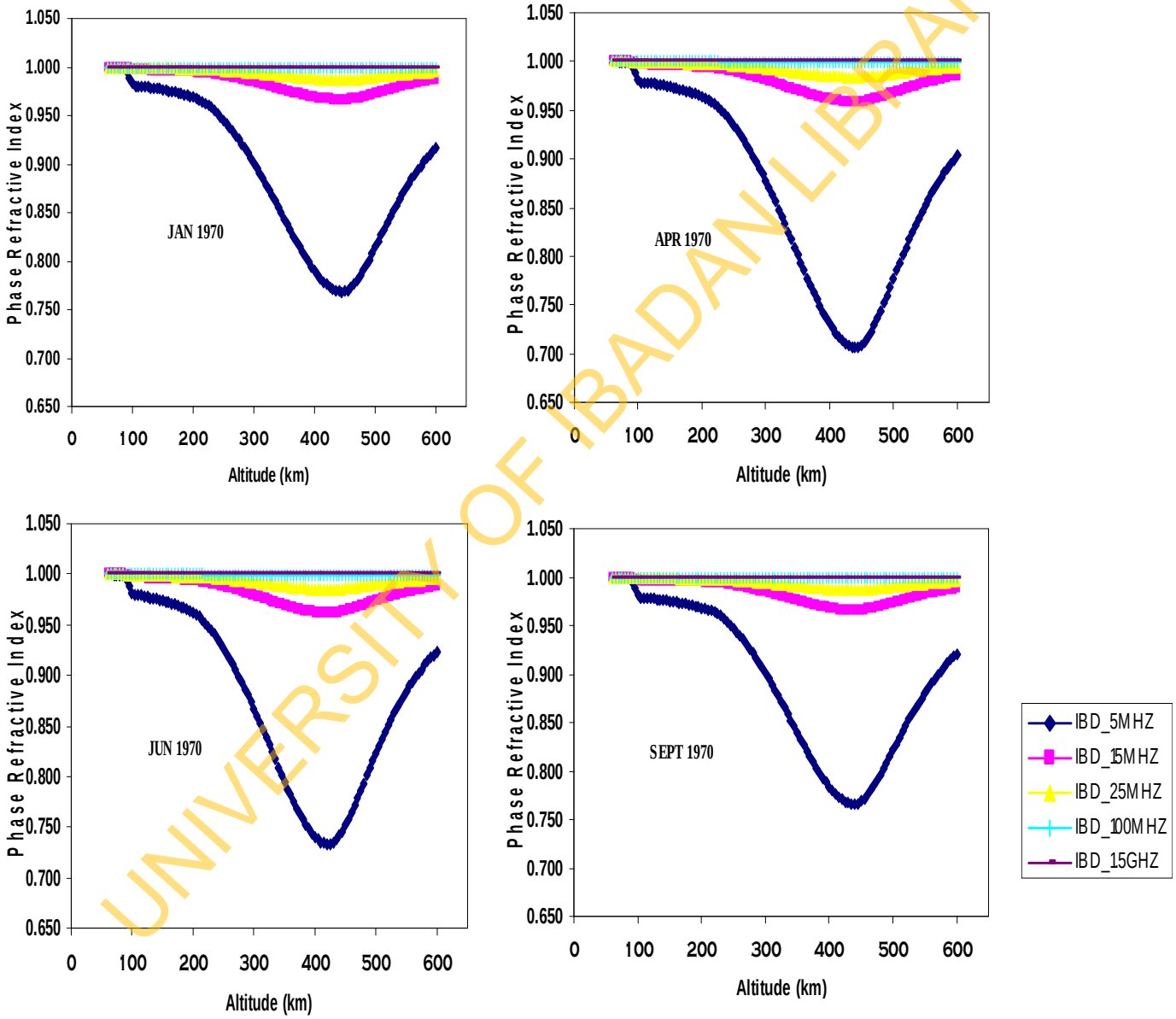

Figure 3. The variability of phase refractive index at Ibadan for different propagating frequencies during high solar activity Rz =104.5, for different seasons.

comprehended by the ionospheric complex phase refractive index as shown in this work for desired ionospheric regions. For vertical propagation of radio signals, this theoretical model can be used for studying,

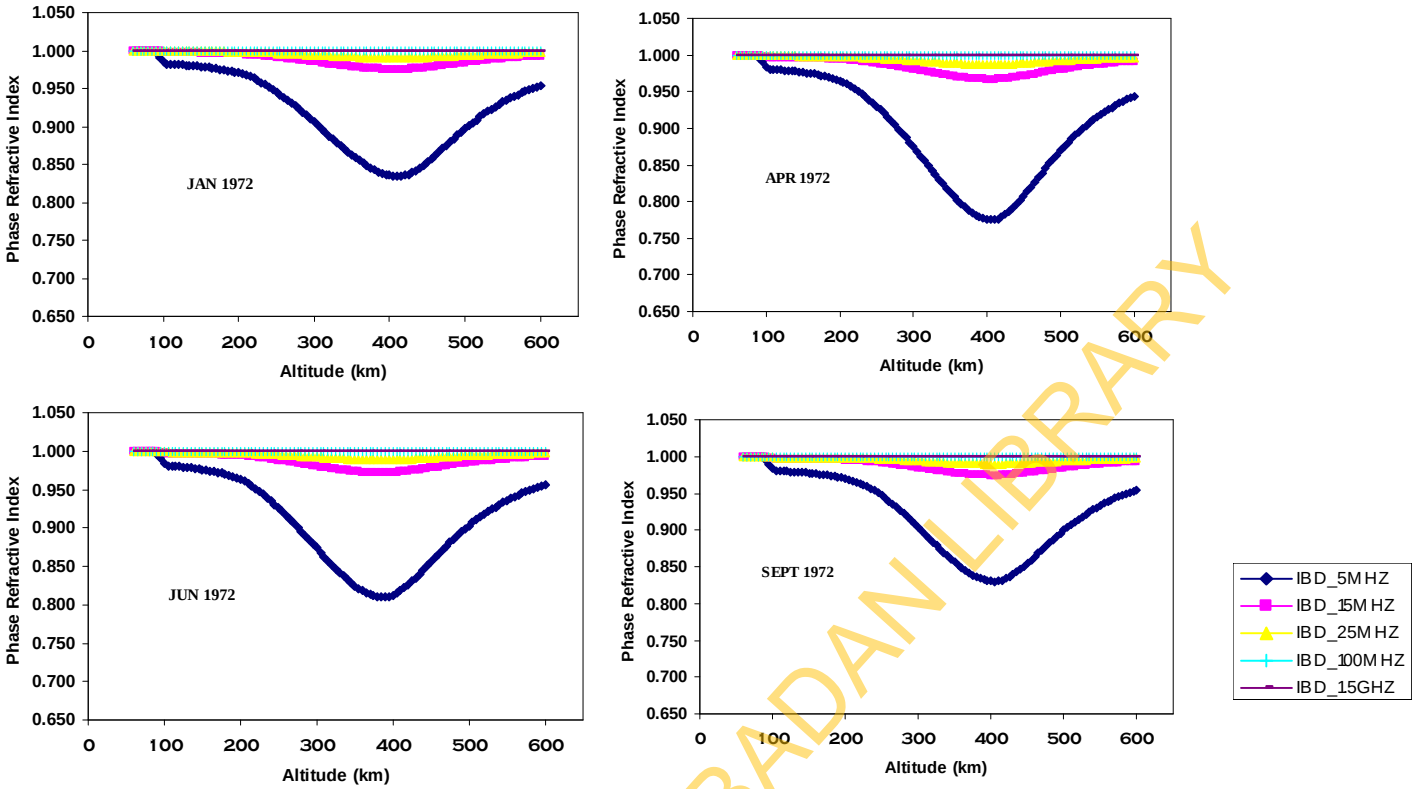

Figure 4. The variability of phase refractive index at Ibadan for different propagating frequencies during moderate solar activity Rz =68.9, for different seasons.

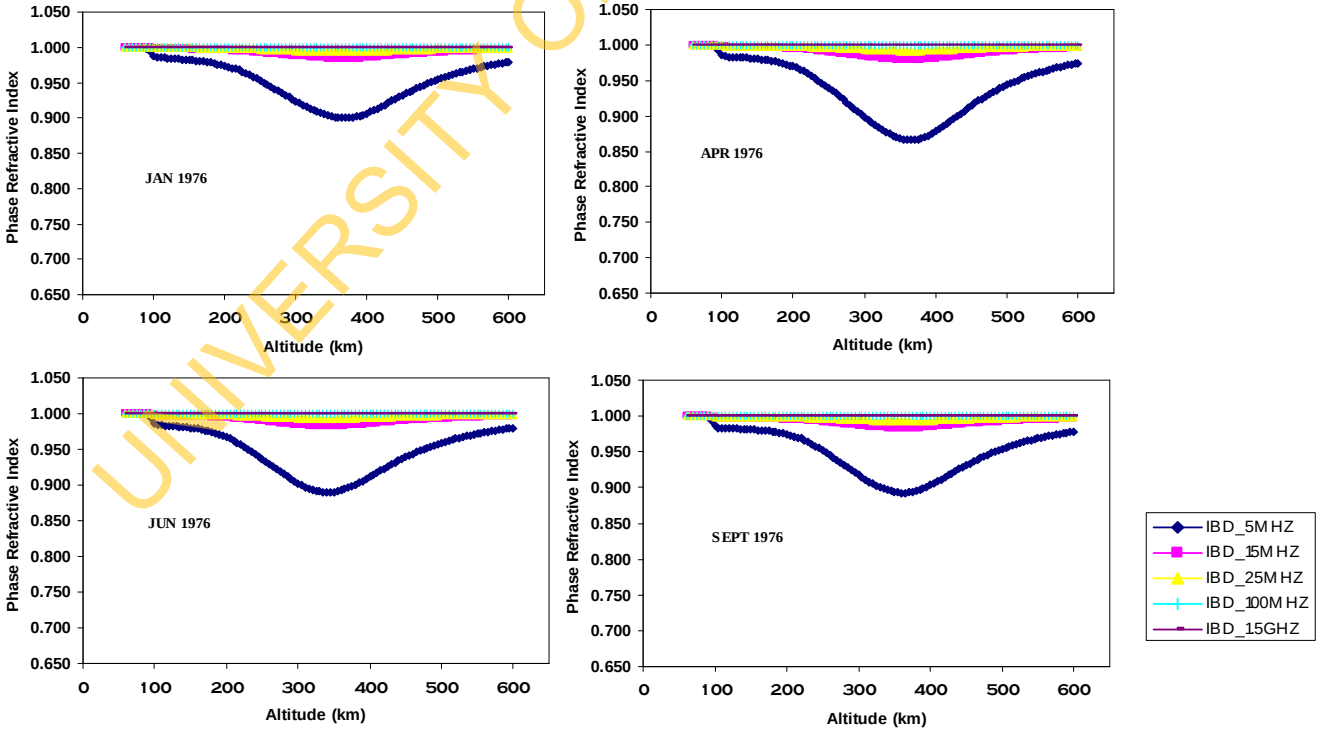

Figure 5. The variability of phase refractive index at Ibadan for different propagating frequencies during low, solar activity Rz =12.6, for different seasons.

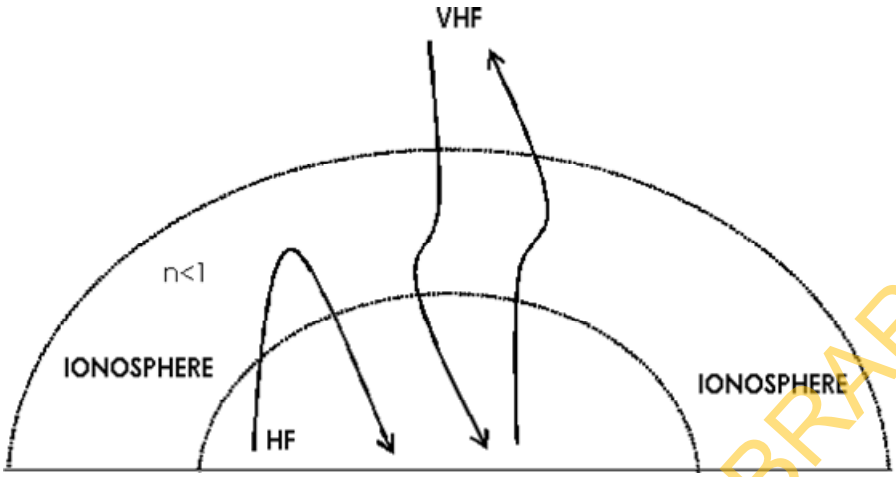

Figure 6. Ionospheric effects on radio wave propagation.

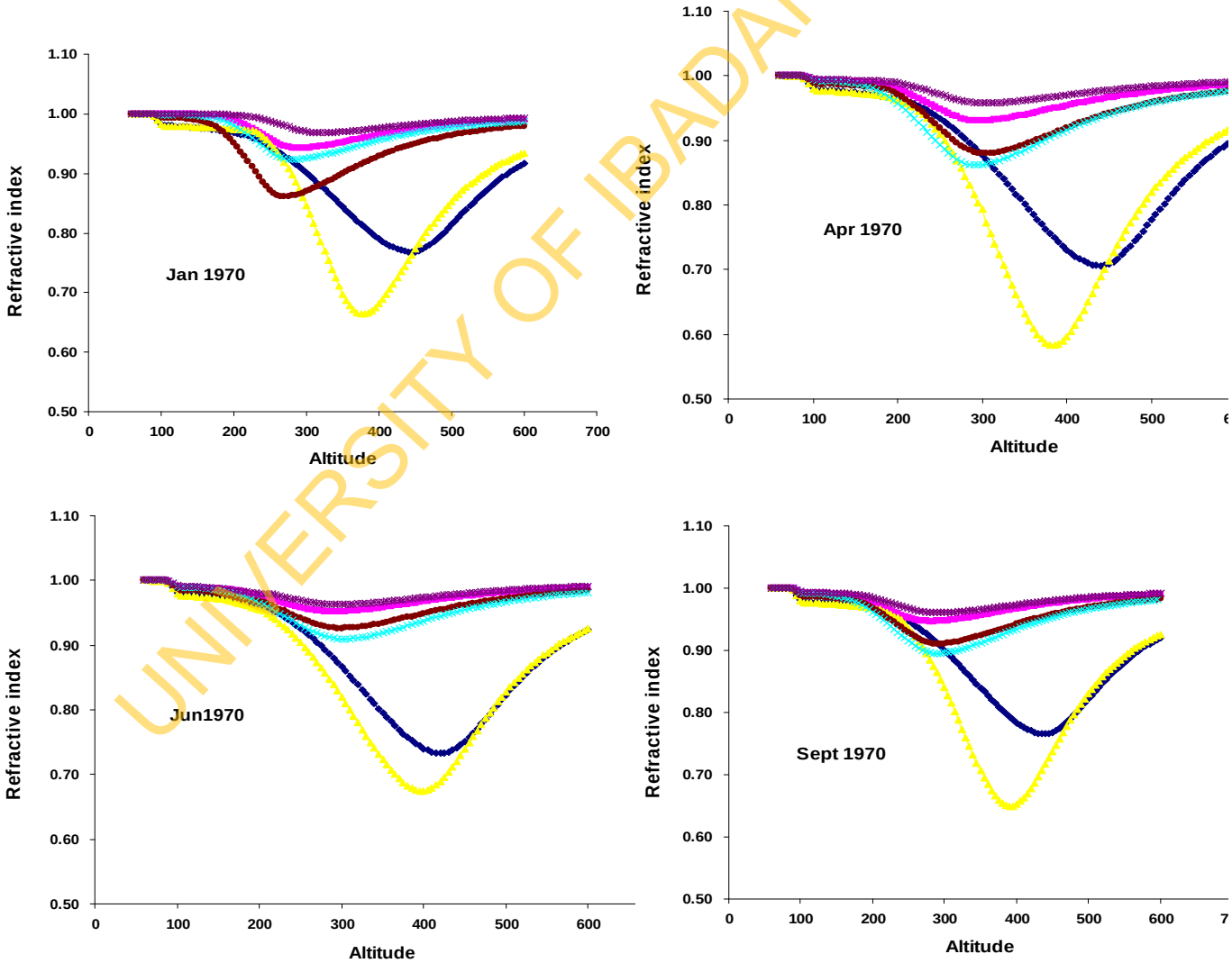

Figure 7. The variability of phase refractive index for the stations for 5 MHz during high solar activity Rz =104.5, for different seasons.

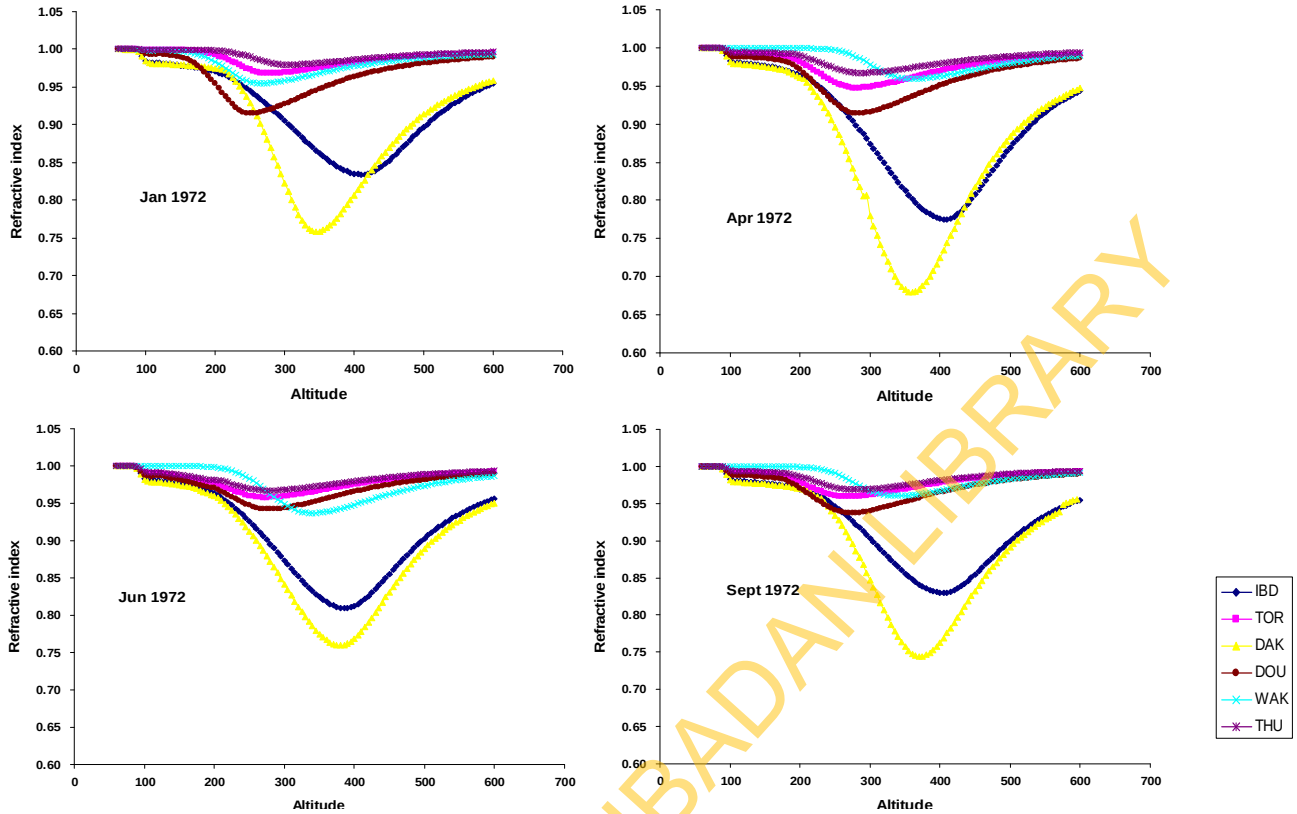

Figure 8. The variability of phase refractive index for the stations for 5 MHz during moderate solar activity Rz =68.9, for different seasons.

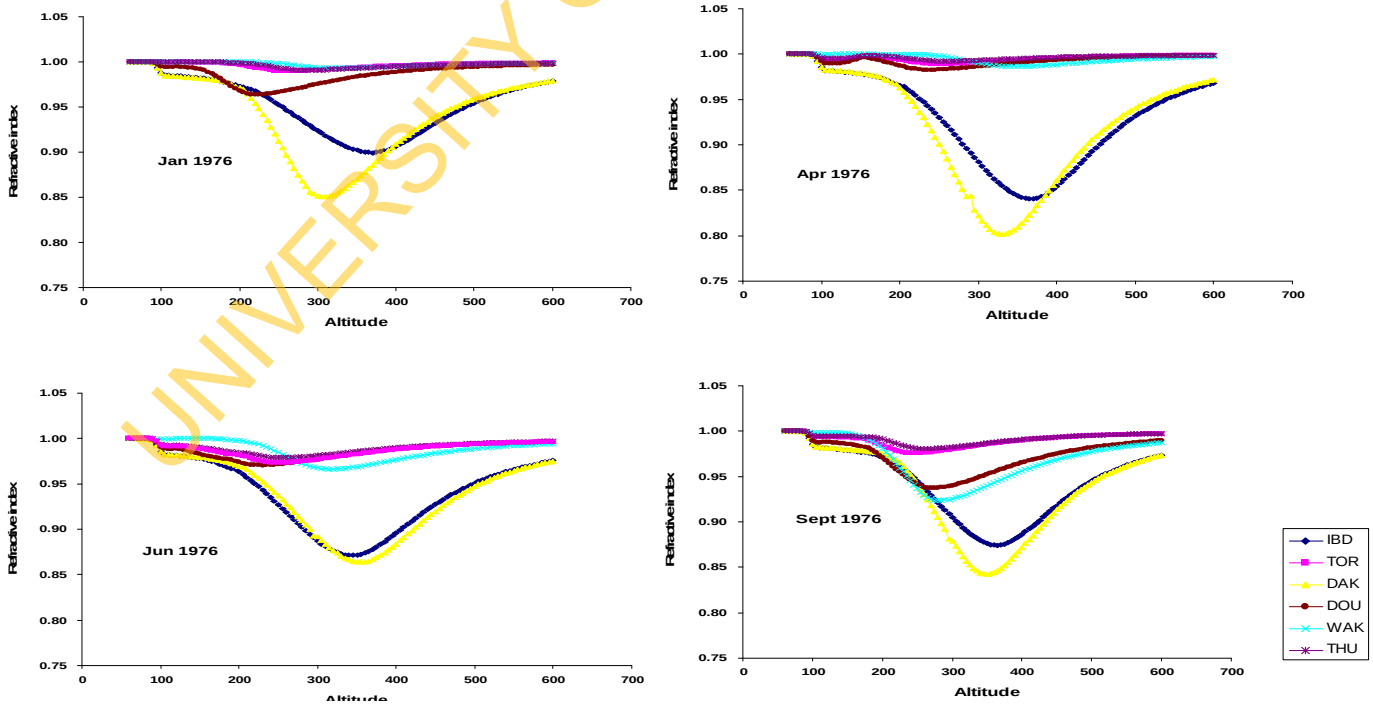

Figure 9. The variability of phase refractive index for the stations for 5 MHz during low solar activity Rz =12.6, for different seasons.

Table 2. Calculated minimum and maximum values of *n* for 5 MHz for all the stations for different solar activities and seasons.

Station		IBD	TOR	DAK	WAK	THU	DOU
Jan-70	Minimum	0.76802339	0.94216517	0.66343797	0.92371808	0.96832522	0.86132612
	Maximum	0.99996124	0.99999982	0.99995804	0.99999931	0.99999913	0.99998577
Apr-70	Minimum	0.70589303	0.93020940	0.58322336	0.86202133	0.95784185	0.87947378
	Maximum	0.99994823	0.99998470	0.99994319	0.99998728	0.99998720	0.99995050
Jun-70	Minimum	0.73290839	0.95166949	0.67463787	0.90947704	0.96316333	0.92622351
	Maximum	0.99994804	0.99996326	0.99994193	0.99997249	0.99996965	0.99994525
Sep-70	Minimum	0.76568026	0.94651578	0.64887943	0.89524184	0.96028747	0.91047246
	Maximum	0.99994624	0.99998313	0.99994099	0.99998689	0.99998566	0.99995043
Jan-72	Minimum	0.83406463	0.96798984	0.75824857	0.95486002	0.97980371	0.91508798
	Maximum	0.99996124	0.99999983	0.99995804	0.99999931	0.99999913	0.99998586
Apr-72	Minimum	0.77504162	0.94760907	0.67910328	0.95933245	0.96710758	0.91418453
	Maximum	0.99995893	0.99998477	0.99995482	0.99999985	0.99998728	0.99996042
Jun-72	Minimum	0.80938005	0.95784215	0.75934221	0.93689090	0.96742142	0.94225252
	Maximum	0.99995849	0.99997076	0.99995376	0.99999902	0.99997583	0.99995652
Sep-72	Minimum	0.82986125	0.95898758	0.74425982	0.96026358	0.96880912	0.93731324
	Maximum	0.99995740	0.99998324	0.99995316	0.99999987	0.99998576	0.99996098
Jan-76	Minimum	0.89957807	0.98998914	0.85062947	0.99329778	0.99084396	0.96371931
	Maximum	0.99997710	0.99999983	0.99997516	0.99999994	0.99999913	0.99998593
Apr-76	Minimum	0.84027822	0.98901473	0.80173685	0.98625039	0.99229456	0.98263330
	Maximum	0.99999595	0.99998482	0.99997328	0.99999988	0.99998731	0.99997672
Jun-76	Minimum	0.87109272	0.97326357	0.86407971	0.96637151	0.97889468	0.97051500
	Maximum	0.99999228	0.99998282	0.99997269	0.99999902	0.99998580	0.99997443
Sep-76	Minimum	0.87425049	0.97578579	0.84246098	0.92371808	0.98073675	0.93731324
	Maximum	0.99999224	0.99998332	0.99997232	0.99999931	0.99998582	0.99996098

investigating and understanding the dynamics of the ionospheric plasmas in term of varying refractive index on radio signals. It yields a robust and a more informative result than the approximated AH model and can be used for better prediction purposes in radio communications through the ionosphere. The calculated high attenuations for the two equatorial regions as compared with other ionospheric regions need further investigation and as well as the ionospheric conductivities of these regions.

ACKNOWLEDGEMENTS

The authors are grateful to the University of Ibadan, for making this research possible by providing the facilities needed for the study; to Dr. Unal Ibrahim of the Inonu University, Malatya, Turkey for his contribution, and to Community Coordinated Modeling Center (CCMC) and Space Physics Interactive Data Resource (SPIDR) for providing data that were used in this work.

Abbreviations: HF, High frequency; **IGRF,** International Geomagnetic Reference Field; **MSIS-E,** mass spectrometer - incoherent scatter extended; **Rz,** smoothed sunspot number; **AH,** Appleton-Hartree; **DAK,** Dakar Station; **DOU,** Dourbes Station; **HF,** High frequency; **IBD**, Ibadan Station; **IGRF**, International Geomagnetic Reference Field; **MSIS-E**, Mass Spectrometer - Incoherent Scatter Extended; **Rz**, Smoothed Sunspot Number; **THU**, Thule Station; **TRO**, Tromso Station; **WAK**, Wakkanai Station.

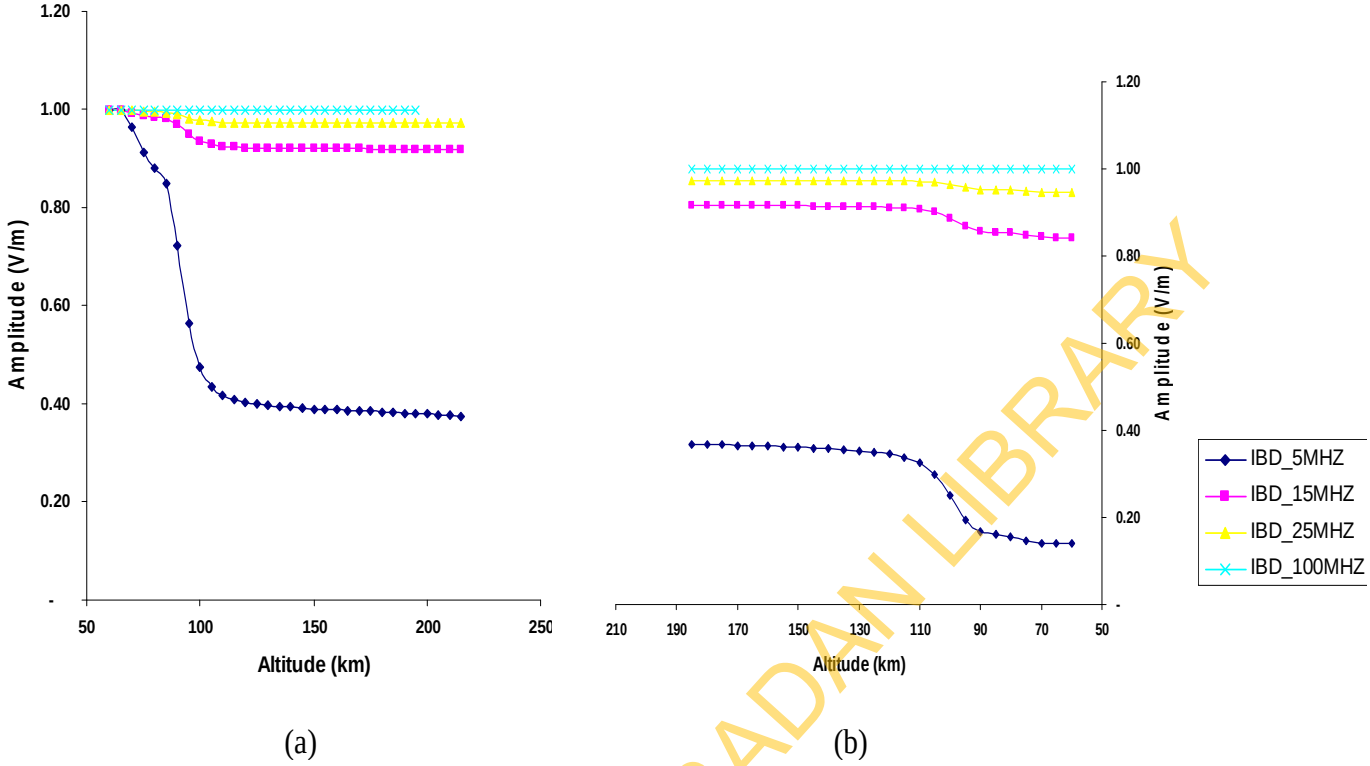

Figure 10. The variation of the amplitude attenuation of 1 V/m with altitude at Ibadan for different propagating frequencies for January 1970; (a) Transmitted signals; (b) Reflected signals.

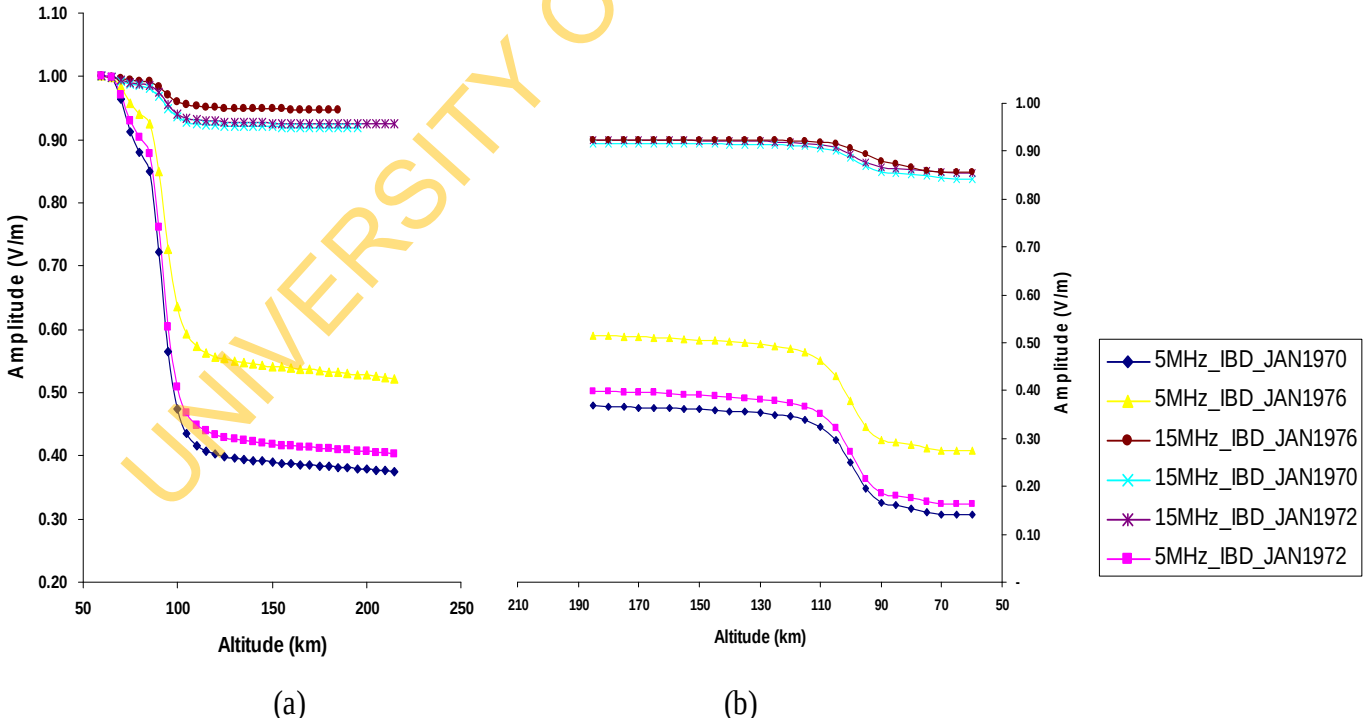

Figure 11. The variation of the amplitude attenuation of 1 V/m with altitude at Ibadan for different propagating frequencies for different solar activities; (a) Transmitted signals; (b) Reflected signals.

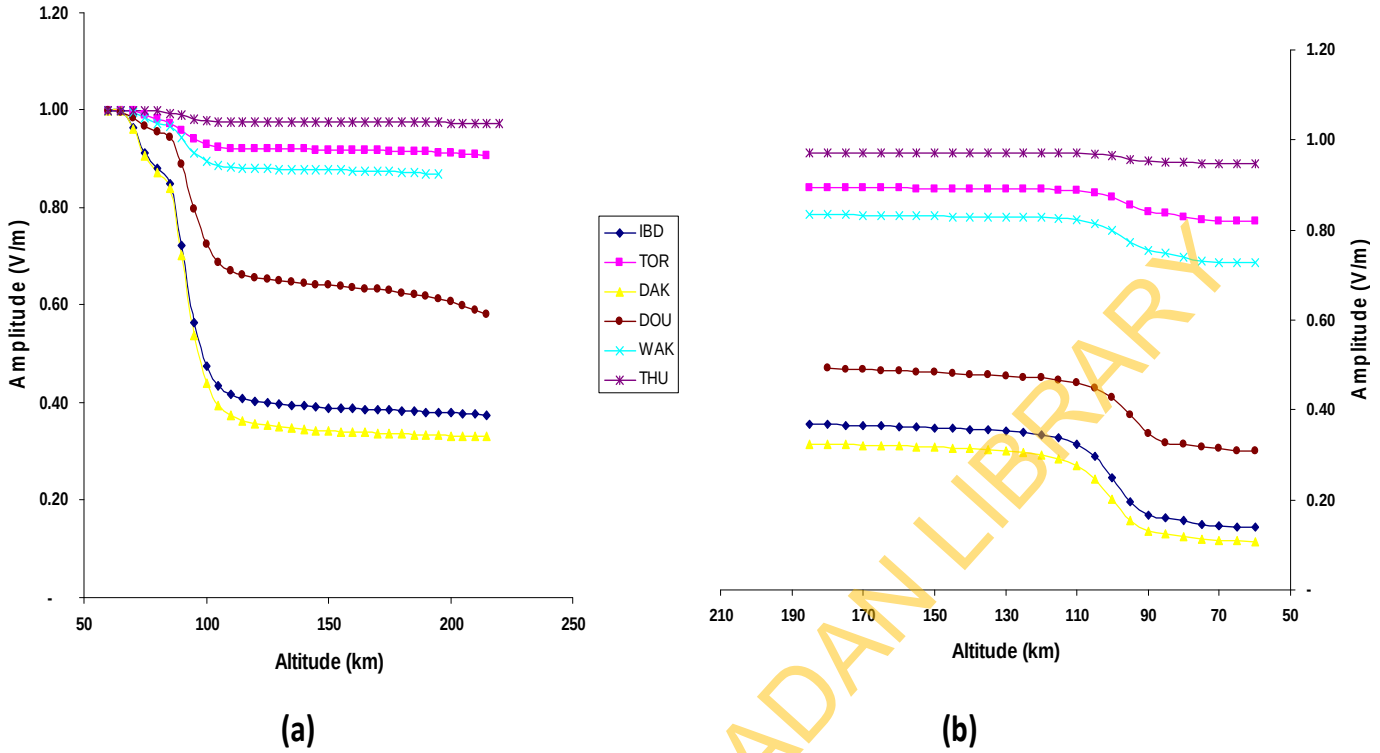

Figure 12. The variation of the attenuation of 1 Vm^{-1} with height for 5 MHz for January 1970: (a) Transmission; (b) Reflection.

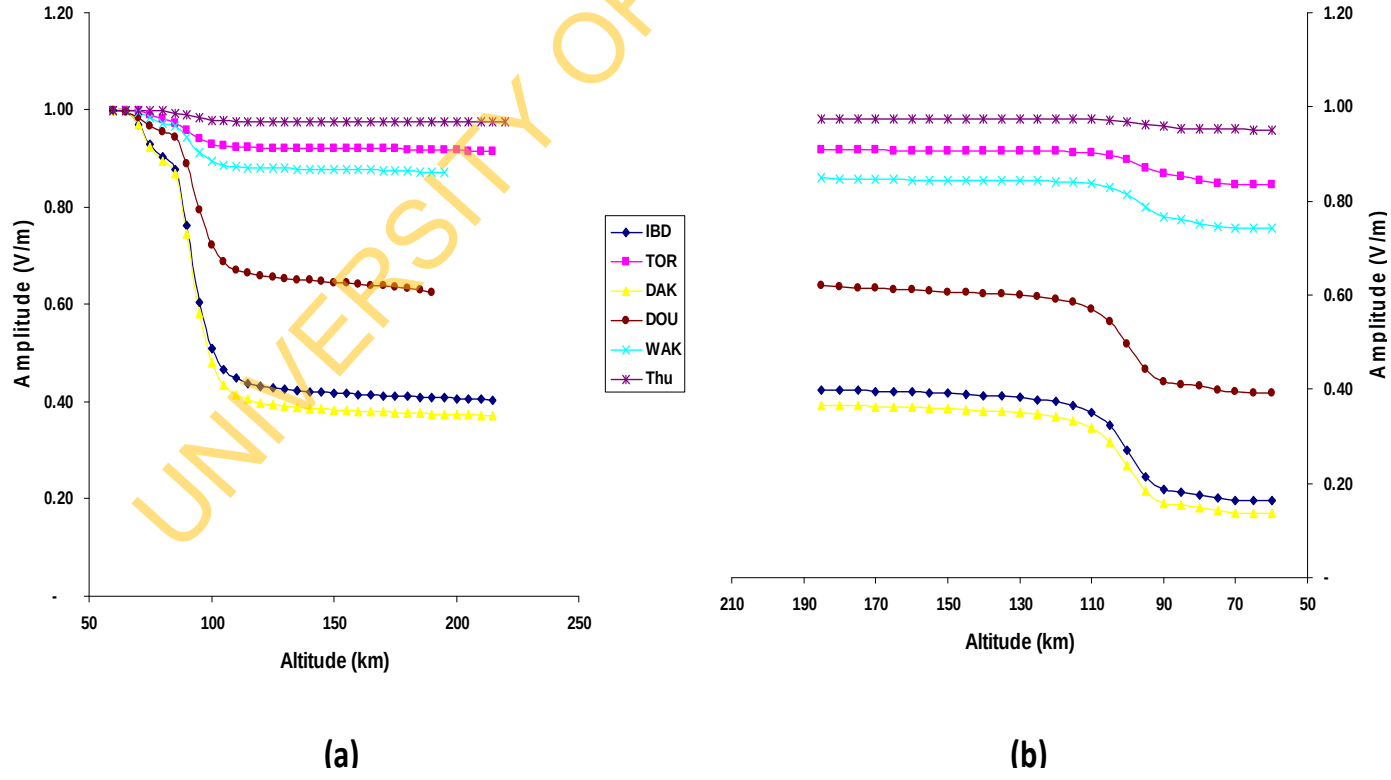

Figure 13. The variation of the attenuation of 1Vm^{-1} with height for 5 MHz for January 1972: (a) Transmission; (b) Reflection.

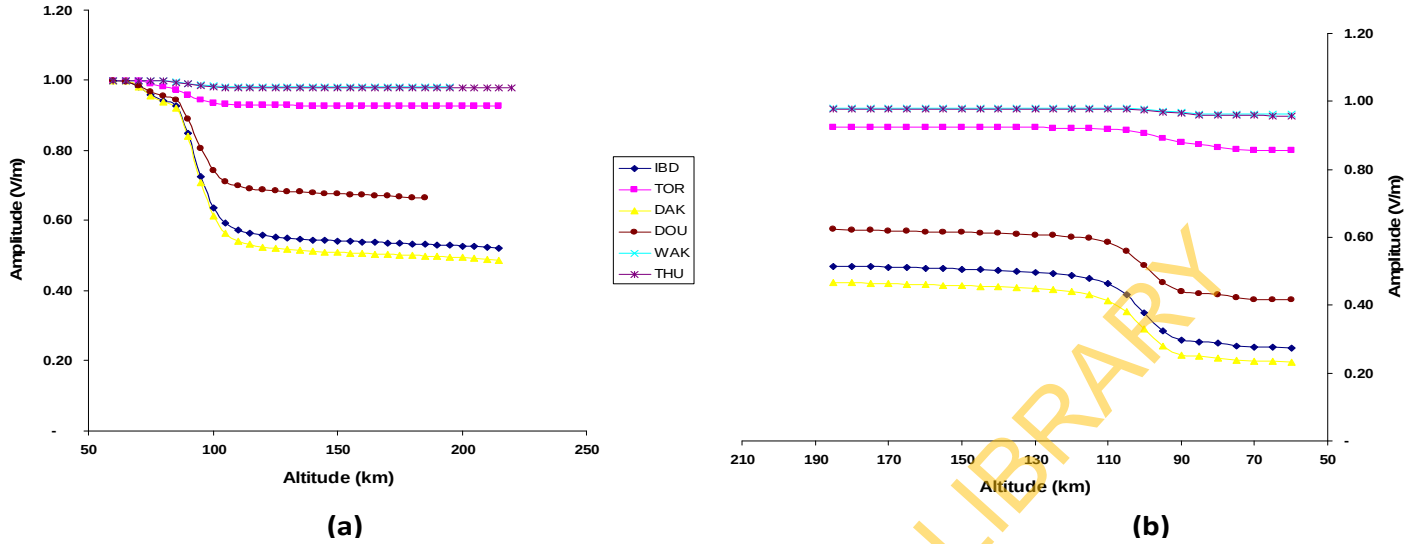

Figure 14. The variation of the attenuation of 1 Vm^{-1} with height for 5 MHz for Jan 1976: (a) Transmission; (b) reflection.

Table 3. The variation of attenuation with solar activity.

1970 (Rz=104.5)	1972 (Rz=68.9)	1976 (Rz=12.6)
Attenuation is very high	Attenuation is high	Attenuation is low

Attenuation is insignificant at VHF and above.

Table 4. The variation of attenuation with ionospheric regions.

Equatorial	Mid-latitude	High-latitude
Attenuation is very high	Attenuation is high	Attenuation is low

Table 5. The variation of attenuation with ionospheric seasons.

December solstice	March equinox	June solstice
Attenuation is low	Attenuation is high	Attenuation is very high

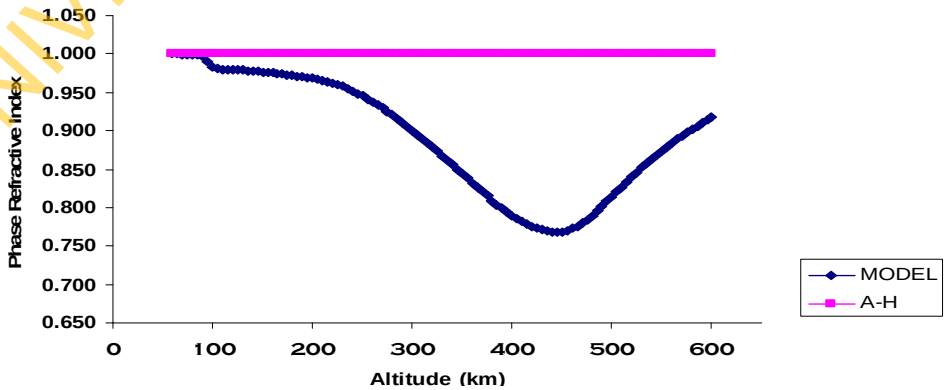

Figure 15. The variability of phase refractive index at Ibadan for 5 MHz for AH model and our model for January 1970.

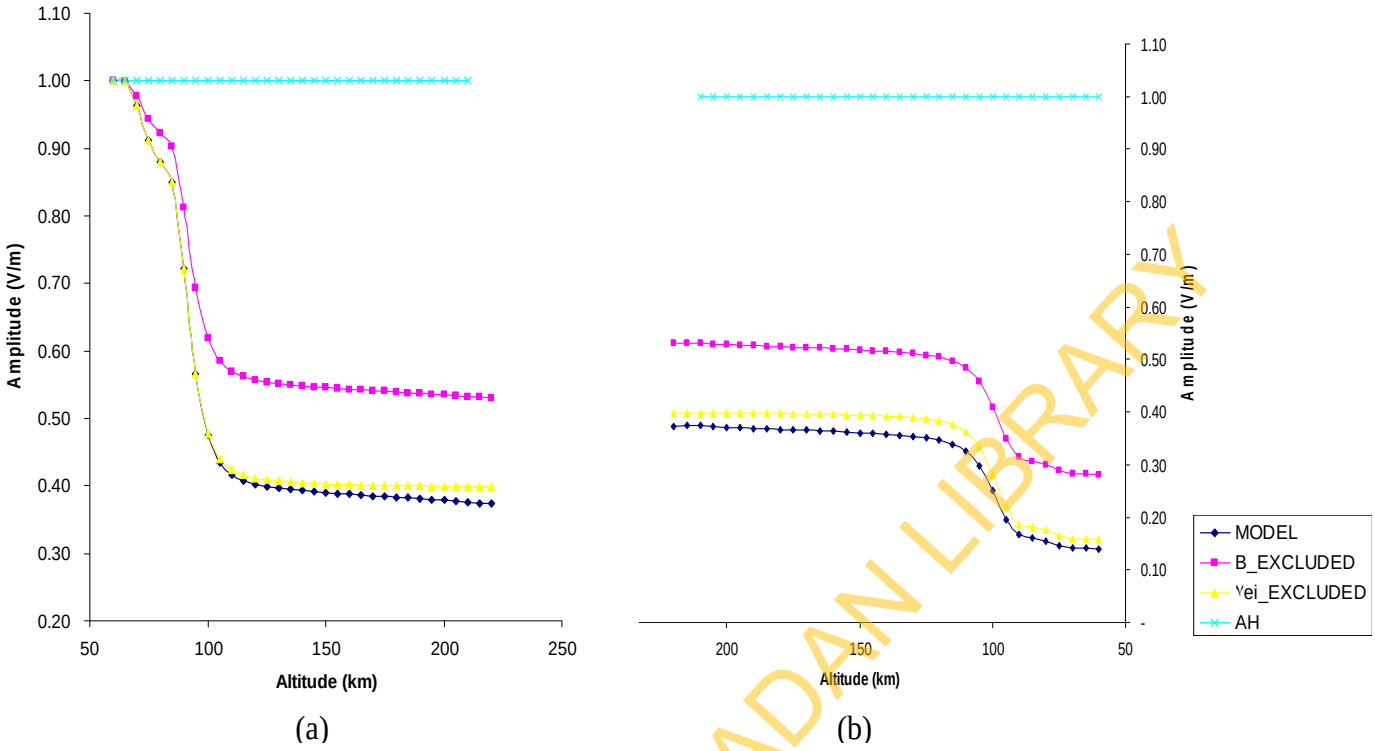

Figure 16. The variation of the amplitude attenuation of 1 V/m with altitude for 5MHz for January 1970 for our model and AH model; (a) Transmitted signals; (b) Reflected signals.

REFERENCES

Aydodu M, Ozcan O (1996). Effects of magnetic declination on refractive index and wave polarization coefficients of electromagnetic waves in mid-latitude ionosphere, Ind. J. Rad. Sp. Phy., 25: 263-270.

Bassiri S, Hajj GA (1993). Higher-Order Ionospheric Effects on the Global Positioning System Observables and Means of Modelling Them. Manuscripta Geodaetica. 18: 280-289.1992.

Baumjohann W, Treumann RA (1999). Basic Space Plasma Physics. Imperial College Press, pp. 52-55.

Bittencourt JA (1986). Fundamentals of plasma physics, Pergamon Press., pp. 245-248.

Bo T (2004). Electromagnetic Field Theory. Uppsala, Sweden.

Budden KG (1988). The propagation of radio waves. Cambridge University Press, pp. 3-4.

Davies K (1990). Ionospheric Radio. Peter Peregrinus Ltd., London, United Kingdom. pp. 9-11.

Habarulema JB (2007). A feasibility study into Total Electron Content prediction using Neural Networks. MSc Thesis, Rhodes University, South Africa. pp. 22-25.

Hunsucker RD (1991). Radio Techniques for Probing the Ionosphere, Springer-Verlag, New-York, pp. 47-48.

Kintner PM, Ledvina BM (2004). The ionosphere, radio navigation, and global navigation satellite systems. Advan. Space Res., 35(5): 788-811.

Komjathy A (1997). Global Ionospheric Total Electron Content Mapping Using the Global Positioning System. Ph.D. dissertation, University of New Brunswick, Fredericton, Canada, p.248.

Langley RB, Komjathy A (1996). High Precision Ionospheric Total Electron Count Mapping Using the Navstar Global Positioning System. Presented at the American Geophysical Union (AGU) Western Pacific Geophysics Meeting, Brisbane, Australia. pp. 23-27.

Liu CH, Yeh KC (1970). Effects of Ionospheric Irregularities on Stabilities of Wave Amplitude and Phase in Space Communication. AGARD Conference Proceedings, 33: 535-544.

Okeke FN, Onwuneme SE, Hanson EA (2009). Investigation of electron density variation in some regions of the Ionosphere at Nsukka, Nigeria. Int. J. Lib. Inf. Sci., 1(2): 012-016.

Oyinloye JO (1975). Radio-wave absorption in the equatorial ionosphere. J. Atmos. Terr. Phy., 37: 1-16.

Oyinloye JO (1988). Equatorial HF radio wave absorption measurements and the IRI. J. Atmos. Terr. Phy., 50: 519-522.

Ratcliffe JA (1959). The magneto-ionic theory and its applications to the ionosphere. Cambridge University Press.

Rishbeth H, Garriott OK (1969). Introduction to ionospheric physics. Academic Press, pp. 134-136.

Siegfried BJ (1973). Physics of Planetary Ionospheres. Germany: Springer-Verlag., pp. 134-136.

Unal I, Ozcan O, Canyilmaz M (2007). Ionospheric absorption of HF radio wave in vertical propagation. Iran. J. Sci Tech, Trans. A, 31: A4.

URL-1 (1999). International Symposium on Advanced Radio Technologies (ISART) web page. Available at http://www.its.bldrdoc.gov/isart/art99/slides99/smi/smi_abs.pdf, p. 1.

URL-2 (2000). GPS world innovation columns web page. Available at http://gauss.gge.unb.ca/gpsworld/gpsworld.july00.pdf, pp. 44-49.

URL-3 (2008). Introduction to Plasma Physics: A graduate level course wab page. Available at http://farside.ph.utexas.edu/teaching/plasma/380.pdf, pp. 105-107.